Resolution of eicosanoid/cytokine storm prevents carcinogen and inflammation-initiated hepatocellular cancer progression

Anna Fishbein[a,b,c,1], Weicang Wang[d,e,1], Haixia Yang[a,b,c,1], Jun Yang[d,e,1], Victoria M. Hallisey[a,b,c,1], Jianjun Deng[a,b,c,1], Sanne M. L. Verheul[a,b,c], Sung Hee Hwang[d,e], Allison Gartung[a,b,c], Yuxin Wang[d,e], Diane R. Bielenberg[f], Sui Huang[g], Mark W. Kieran[h,i,2], Bruce D. Hammock[d,e,1,3], and Dipak Panigrahy[a,b,c,1,3]

[a]Center for Vascular Biology Research, Beth Israel Deaconess Medical Center, Harvard Medical School, Boston, MA 02215; [b]Department of Pathology, Beth Israel Deaconess Medical Center, Harvard Medical School, Boston, MA 02215; [c]Cancer Center, Beth Israel Deaconess Medical Center, Harvard Medical School, Boston, MA 02215; [d]Department of Entomology and Nematology, University of California, Davis, CA 95616; [e]University of California, Davis Comprehensive Cancer Center, University of California, Davis, CA 95616; [f]Vascular Biology Program, Boston Children's Hospital, Harvard Medical School, Boston, MA 02115; [g]Institute for Systems Biology, Seattle, WA 98109; [h]Division of Pediatric Oncology, Dana-Farber Cancer Institute, Harvard Medical School, Boston, MA 02215; and [i]Department of Pediatric Hematology/Oncology, Boston Children's Hospital, Harvard Medical School, Boston, MA 02115

Contributed by Bruce D. Hammock, June 11, 2020 (sent for review April 21, 2020; reviewed by Kenneth Honn and Ann C. Skulas-Ray)

Toxic environmental carcinogens promote cancer via genotoxic and nongenotoxic pathways, but nongenetic mechanisms remain poorly characterized. Carcinogen-induced apoptosis may trigger escape from dormancy of microtumors by interfering with inflammation resolution and triggering an endoplasmic reticulum (ER) stress response. While eicosanoid and cytokine storms are well-characterized in infection and inflammation, they are poorly characterized in cancer. Here, we demonstrate that carcinogens, such as aflatoxin B_1 (AFB_1), induce apoptotic cell death and the resulting cell debris stimulates hepatocellular carcinoma (HCC) tumor growth via an "eicosanoid and cytokine storm." AFB_1-generated debris up-regulates cyclooxygenase-2 (COX-2), soluble epoxide hydrolase (sEH), ER stress-response genes including *BiP*, *CHOP*, and *PDI* in macrophages. Thus, selective cytokine or eicosanoid blockade is unlikely to prevent carcinogen-induced cancer progression. Pharmacological abrogation of both the COX-2 and sEH pathways by PTUPB prevented the debris-stimulated eicosanoid and cytokine storm, down-regulated ER stress genes, and promoted macrophage phagocytosis of debris, resulting in suppression of HCC tumor growth. Thus, inflammation resolution via dual COX-2/sEH inhibition is an approach to prevent carcinogen-induced cancer.

cell death | carcinogenesis | soluble epoxide hydrolase | inflammation resolution | bioactive lipid

Aflatoxins, a group of natural carcinogens, represent one of the critical causes of hepatocellular carcinoma (HCC), the second leading cause of cancer mortality worldwide. Aflatoxin B_1 (AFB_1), a mycotoxin produced by *Aspergillus* fungi, is a contaminant of a large portion of the world's food supply, causing over 5 billion people to be at high risk for HCC (1, 2). Aflatoxins may play a causative role in 4.6 to 28.2% of all HCC cases worldwide (3). While AFB_1-induced DNA damage mediates HCC, AFB_1-derived DNA adducts alone may not be sufficient to cause and promote HCC or predict its progression (4–6). In addition to DNA damage or DNA adduct formation, other key characteristics of carcinogens include their ability to induce oxidative stress, promote chronic inflammation, be immunosuppressive, and stimulate angiogenesis (7–9). Aflatoxins are also cytotoxic and various types of cell death can induce lineage switching of hepatocytes to produce HCC or intrahepatic cholangiocarcinoma, supporting nongenetic mechanisms in tumorigenesis (10). HCC ensues in the presence of excessive hepatic apoptosis and nonresolving inflammation in the tumor microenvironment (10, 11). Apoptotic cell death stimulates production of tumor-promoting eicosanoids, including cyclooxygenase (COX)-derived prostaglandins, through the arachidonic acid pathway in the tumor microenvironment (12–15). Aflatoxins trigger proinflammatory cytokines (e.g., TNF-α and IL-6) as well as caspase activation, leading to apoptotic cell death of multiple cell types, including hepatocytes, lymphocytes, splenocytes, macrophages, and endothelial cells (16–18). AFB_1 can also negatively impact the innate immune defense by impairing macrophage functions, such as phagocytosis (19), a critical process in the resolution of inflammation (15, 20, 21).

While environmental carcinogens can cause cancer, their nongenotoxic mechanisms are not well understood. Cell death ("debris")-mediated hyperinflammation generated by cytotoxic drugs stimulates the growth of surviving tumor cells via a cytokine storm of proinflammatory and proangiogenic mediators (14, 15, 22, 23). Chronic inflammation and proinflammatory cytokines cause hyperplasia, oxidative stress, and act synergistically

Significance

Eicosanoid and cytokine storms are poorly characterized in cancer. Our study demonstrates the environmental carcinogen aflatoxin B_1 (AFB_1) promotes hepatocellular carcinoma (HCC) by triggering a debris-stimulated proinflammatory and proangiogenic "eicosanoid and cytokine storm" in the tumor microenvironment. The dual COX-2/sEH inhibitor PTUPB prevents AFB_1-stimulated HCC growth by increasing macrophage phagocytosis of debris and suppressing the eicosanoid and cytokine storm, thus promoting resolution of inflammation. Enhancing endogenous clearance of debris via eicosanoid regulation, such as dual inhibition of COX-2/sEH, is a strategy to stifle inflammation and thus suppress tumor progression driven by carcinogens. sEH and dual COX-2/sEH inhibitors are in clinical development for multiple inflammatory diseases and thus may be rapidly translated for the prevention and treatment of carcinogen-induced cancers.

Author contributions: A.F., W.W., B.D.H., and D.P. designed research; A.F., W.W., H.Y., J.Y., V.M.H., J.D., S.M.L.V., S.H.H., Y.W., and D.R.B. performed research; A.F., W.W., S.H.H., A.G., S.H., M.W.K., and D.P. analyzed data; and A.F., W.W., A.G., S.H., M.W.K., B.D.H., and D.P. wrote the paper.

Reviewers: K.H., Wayne State University; and A.C.S.-R., University of Arizona.

The authors declare no competing interest.

[1]A.F., W.W., H.Y., J.Y., V.M.H., J.D., B.D.H., and D.P. contributed equally to this work.

[2]Present address: Pediatric Oncology, Bristol-Myers Squibb, Lawrenceville, NJ 08648.

[3]To whom correspondence may be addressed. Email: bdhammock@ucdavis.edu or dpanigra@bidmc.harvard.edu.

This article contains supporting information online at https://www.pnas.org/lookup/suppl/doi:10.1073/pnas.2007412117/-/DCSupplemental.

First published August 14, 2020.

with DNA damage to drive mutations and carcinogenesis (24–27). Carcinogens induce reactive oxygen and nitrogen species, resulting in oxidative stress and inflammation (28). Activation of the mitochondrial apoptotic pathway in hepatocytes generates reactive oxygen species (ROS), leading to oxidative damage and liver tumorigenesis (29). Inflammatory cells and cancer cells generate free radicals and soluble mediators, such as metabolites of arachidonic acid, cytokines, and chemokines, which act by further producing reactive species (27). These mediators, including proinflammatory cytokines (e.g., IL-6, CCL2/MCP-1, and TNF-α), are stimulated by carcinogens and correlate with poor patient survival. Neutralization of these proinflammatory cytokines has been demonstrated to suppress carcinogen-induced cancer and HCC progression (30, 31). AFB_1-induced HCC is suppressed by a potent antiinflammatory, synthetic triterpenoid, which only partially reduces the AFB_1 adduct burden (4). Activation of endogenous inflammation resolution programs counterregulates a series of proinflammatory cytokines via clearance of debris (15, 20, 21, 32), eliminates micrometastases, and prevents tumor recurrence (33).

Selective cytokine or eicosanoid pathway blockade by antiinflammatory agents, such as COX-2 selective inhibitors (coxibs), have resulted only in transient antiinflammatory and antitumor activity in patients (34–41). Coxibs cause a shunting of arachidonic acid metabolism to cytochrome P450 (CYP450) and lipoxygenase (LOX) pathways, which counteracts the antitumor

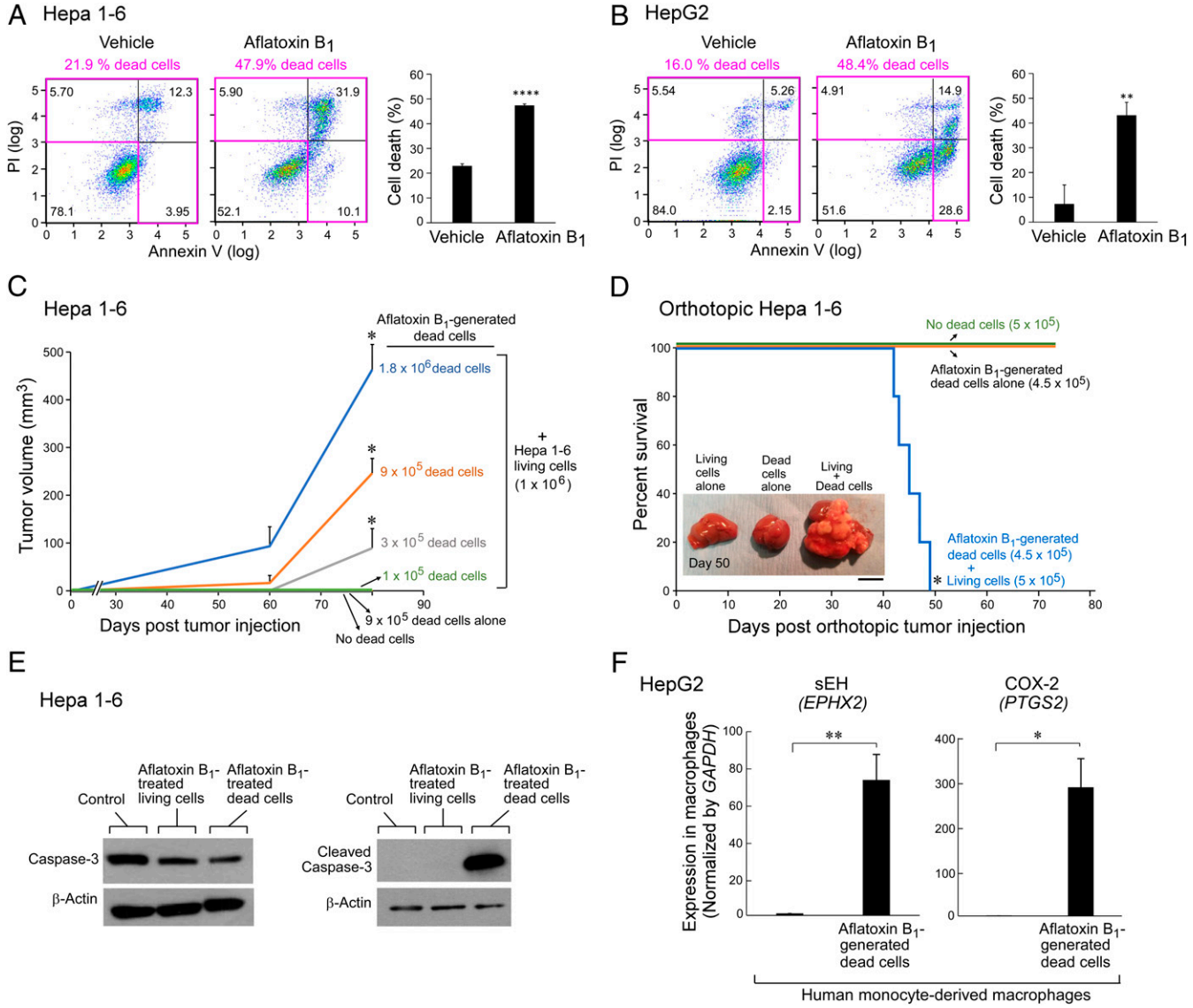

Fig. 1. AFB_1-generated cell death stimulates HCC via up-regulation of sEH and COX-2. Annexin V/PI analysis of (*A*) Hepa 1-6 murine and (*B*) HepG2 human HCC tumor cells treated with AFB_1 (25 μM, 48 h) compared to vehicle. Quadrants containing dead tumor cells are outlined in pink. Bar graphs represent means of percent cell death ±SEM. $n = 3$ per group. $^{**}P < 0.01$, $^{****}P < 0.0001$ vs. vehicle. (*C*) Hepa 1-6 tumor growth stimulated by AFB_1-generated dead cells coinjected with a subthreshold inoculum of living cells. $n = 5$ to 15 mice per group. The two-tailed unpaired Student's *t* test was used for final tumor measurements throughout. $^{*}P < 0.05$ vs. 10^6 living cells alone (no dead cells). (*D*) Percent survival of mice coinjected orthotopically into the liver with AFB_1-generated Hepa 1-6 dead cells and a subthreshold inoculum of Hepa 1-6 living cells. $n = 5$ mice per group. Kaplan–Meier analysis indicated significantly shortened survival of mice injected with a combination of dead and living cells as depicted by the area under the Kaplan–Meier survival curves. $^{*}P < 0.05$. (Scale bar, 1 cm.) (*E*) Western blot analysis of caspase-3 and cleaved caspase-3 expression in killed and surviving Hepa 1-6 tumor cells treated with AFB_1 (25 μM, 48 h) or vehicle. Control = vehicle-treated Hepa 1-6 living cells. Levels of β-actin demonstrate protein loading. (*F*) Gene expression of sEH (*EPHX2*) and COX-2 (*PTGS2*) in human monocyte-derived macrophages coincubated with AFB_1-generated HepG2 dead cells; analyzed by qPCR and normalized by *GAPDH*. $n = 3$ per group. $^{*}P < 0.05$, $^{**}P < 0.01$ vs. control.

activity of COX-2 inhibition (42, 43). Whereas standard antiinflammatory agents, such as steroids, coxibs, and selective cytokine antagonists do not clear debris and can be "resolution toxic" (20, 44, 45), CYP450-derived epoxyeicosatrienoic acids (EETs) promote the clearance of cellular debris by local macrophages and activate antiinflammatory programs (46–50). EETs are endogenously produced small-molecule lipid autacoid mediators that act as autocrine or paracrine factors to regulate inflammation and angiogenesis (46, 50). While EETs stimulate the production of proresolution lipoxins and macrophage phagocytosis of debris (47, 48, 51, 52), their specific role in inflammation resolution in cancer is poorly characterized. Moreover, EETs are rapidly metabolized in the body by soluble epoxide hydrolase (sEH) to their corresponding dihydroxyeicosatrienoic acids (DiHETEs). Inhibition of sEH can stabilize eicosanoids, such as EETs and other epoxy-fatty acids, which stimulate the endogenous production of proresolving lipid mediators, such as lipoxins, to trigger the resolution of inflammation (53, 54). Deficiency of lipoxin A4 production is associated with increased sEH, which can result in impaired resolution (53, 55). sEH inhibitors can also suppress endoplasmic reticulum (ER) stress and hepatic fibrosis, a risk factor for HCC (56). In fact, the targeted antitumor agent sorafenib, widely used for advanced HCC treatment, is a potent sEH inhibitor (57, 58).

In particular, sEH inhibitors synergize with coxibs to reduce protumorigenic mediators while ameliorating the adverse cardiovascular and gastrointestinal side effects associated with coxibs (59–61). Dual COX-2/sEH inhibitors [e.g., 4-(5-phenyl-3-{3-[3-(4-trifluoromethyl-phenyl)-ureido]-propyl}-pyrazol-1-yl) benzenesulfonamide (PTUPB)] inhibit various inflammation-driven diseases, including cancer, fibrosis, sepsis, fatty liver disease, diabetes, allergic inflammation, and neurodegenerative diseases by counter-regulating multiple proinflammatory cytokines and inhibiting inflammasome activation (14, 61–68). PTUPB may act as a "surge protector" against cancer therapy-induced protumorigenic cytokines and bioactive lipid mediators in the tumor microenvironment to prevent tumor recurrence (14). Thus, dual COX-2/sEH inhibition may have clinical implications for use in combination with cytotoxic cancer therapies to alleviate debris-mediated inflammation (14). PTUPB potently inhibits hepatosteatosis and improves high-fat diet-induced nonalcoholic fatty liver disease (NAFLD) (63). Both COX-2 and sEH are up-regulated in the liver of NAFLD (63). NAFLD and nonalcoholic steatohepatitis, characterized by unresolved chronic inflammation associated with fibrosis, cirrhosis, and oxidative stress, are highly prevalent world-wide and are major causes of HCC (69). Failure of resolution of inflammation, including impaired debris clearance, is an emerging hallmark of cancer and other inflammation-driven diseases (11, 15, 20, 21, 32, 45, 70–75). Thus, we hypothesize that dual COX-2/sEH inhibition may stimulate inflammation resolution that is disrupted by carcinogens such as aflatoxins.

Here, we demonstrate that tumor cells killed by AFB_1 stimulate primary HCC growth when coinjected with a subthreshold (nontumorigenic) inoculum of tumor cells via a macrophage-derived "eicosanoid and cytokine storm" of proinflammatory and proangiogenic mediators. AFB_1-generated debris up-regulates the expression of *PTGS2* (encoding COX-2), *EPHX2* (encoding sEH), and ER stress-response genes (e.g., *C/EBP-homologous protein* [*CHOP*], *binding Ig protein* [*BiP*], and *protein disulfide isomerase 1* [*PDI*]) in debris-stimulated macrophages. We demonstrate that combined pharmacological abrogation of the COX-2 and sEH-mediated eicosanoid pathways via PTUPB prevents AFB_1-induced HCC progression. PTUPB counter-regulates the cytokine storm, including TNF-α, MIP-1α/CCL3, MIP-1β/CCL4, IL-1ra/IL-1F3, MIP-2/CXCL2, serpin E1/PAI-1, and IL-8/CXCL8, by macrophages stimulated with AFB_1-generated debris. Dual COX-2/sEH inhibition stimulates macrophage phagocytosis of AFB_1-generated debris and suppresses the up-regulation of ER stress-response genes in debris-stimulated macrophages. Dual COX-2/sEH inhibition may provide a strategy to address the toxicities and limitations of COX-2 inhibitors in clinical cancer trials. Thus, dual COX-2/sEH inhibition may be a host-directed therapeutic approach to the treatment of carcinogen-induced cancers by targeting the innate immune response via inflammation resolution.

Results

AFB_1-Generated and Caspase-3–Mediated Cell Death Stimulates HCC via Up-Regulation of sEH and COX-2. To evaluate whether AFB_1-generated debris is biologically relevant in liver cancer, we developed carcinogen debris-stimulated HCC models. We confirmed the generation of cell death (apoptotic cells, necrotic cells, and cell fragments; hereafter referred to as "debris") in cell cultures treated with AFB_1 via flow cytometry analysis of annexin V/propidium iodide (PI)-stained cells, and counted the number of dead cell bodies as a surrogate quantity for titrating its tumor-stimulatory potency. AFB_1 increased cell death of Hepa 1-6 and HepG2 HCC tumor cells by 2.2-fold and 3.0-fold, respectively (Fig. 1 *A* and *B*). AFB_1-generated dead cells were collected and coinjected with a subthreshold (nontumorigenic) inoculum of living tumor cells into mice (Fig. 1 *C* and *D*). A low number of injected living tumor cells mimics tumor dormancy or minimal tumor growth (15, 33). In a widely used HCC model (58), AFB_1-generated Hepa 1-6 debris potently stimulated Hepa 1-6 HCC tumor growth (Fig. 1*C*). Increasing the amount of AFB_1-generated Hepa 1-6 debris (10^5, 3×10^5, 9×10^5, or 1.8×10^6 dead cells) coinjected with Hepa 1-6 (10^6 living cells) resulted in accelerated tumor growth in a dose-dependent manner compared to mice injected with living cells alone or dead cells alone (Fig. 1*C*). Tumor cell debris alone did not produce any visible tumors at 80 d postinjection (Fig. 1*C*). AFB_1-generated debris also stimulated tumor dormancy escape and shortened survival in an orthotopic HCC (Hepa 1-6) model compared to mice injected with a subthreshold inoculum of living tumor cells alone (Fig. 1*D*). Debris implanted orthotopically into the liver without living tumor cells did not affect survival (Fig. 1*D*).

Apoptosis-mediated caspase-3 activation stimulates wound healing and tissue regeneration via the "Phoenix Rising" pathway (76). Moreover, therapy-generated apoptotic cell death can stimulate a caspase-3–mediated arachidonic acid pathway, increasing production of PGE_2 (12, 13). Therefore, we determined whether debris generated by AFB_1 could activate caspase-3. Indeed, AFB_1-generated dead cells up-regulated cleaved caspase-3 expression, as opposed to caspase-3, via Western blot analysis, confirming that apoptotic cells activate caspase-3 following AFB_1 exposure (Fig. 1*E*). We next determined whether eicosanoid pathway enzymes are stimulated by AFB_1-generated debris. Gene-expression levels of *EPHX2* (sEH) and *PTGS2* (COX-2) were up-regulated in human monocyte-derived macrophages stimulated with AFB_1-generated HepG2 tumor cell debris (Fig. 1*F*).

Cytokine Storm Triggered by Carcinogen Debris-Stimulated Macrophages Is Prevented by Dual Eicosanoid Pathway Inhibition. Chemotherapy-generated debris can trigger a storm of proinflammatory and proangiogenic cytokines (14, 15, 22). Similarly, AFB_1-generated debris stimulated a proinflammatory and proangiogenic "cytokine storm," including MIP-2/CXCL2, TNF-α, CCL2/MCP-1, G-CSF, and IGFBP-1, by RAW 264.7 murine macrophages (Fig. 2 *A–C*). We next assessed the release of cytokines by RAW 264.7 murine macrophages treated with a dual COX-2/sEH inhibitor (PTUPB) or vehicle prior to stimulation with AFB_1-generated Hepa 1-6 debris. PTUPB (5 μM) prevented the proinflammatory and proangiogenic cytokine storm released by macrophages (Fig. 2 *A–C*). These cytokines were macrophage-derived as only traces of cytokines were detected in conditioned medium of debris alone without macrophages (Fig. 2).

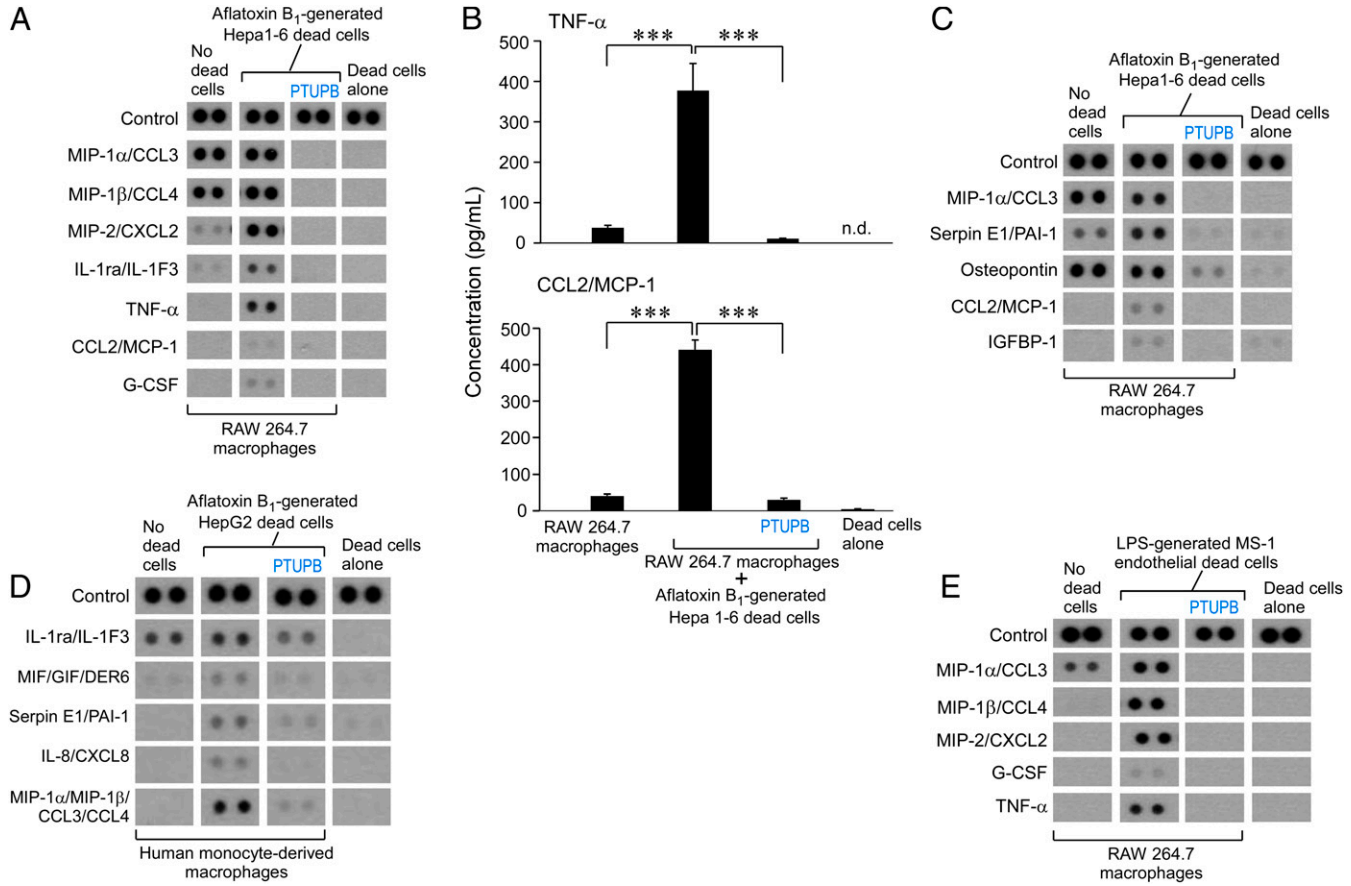

Fig. 2. Cytokine storm triggered by carcinogen debris-stimulated macrophages is prevented by dual eicosanoid pathway inhibition. (*A–C*) Inflammatory and angiogenic cytokine array of conditioned media from RAW 264.7 murine macrophage treated with vehicle or PTUPB (5 μM, 2 h) and stimulated with AFB_1-generated Hepa 1-6 tumor cell debris vs. debris alone without macrophages. ELISA quantification of TNF-α and CCL2/MCP-1 released by RAW 264.7 macrophages treated with vehicle or PTUPB (5 μM, 2 h) and stimulated with AFB_1-generated Hepa 1-6 tumor cell debris. Data are presented as means (pg/mL) ± SEM. $n = 7$ per group; 3 biological repeats. ***$P < 0.001$. n.d., not detectable. (*D*) Inflammatory cytokine array of conditioned media from human monocyte-derived macrophages treated with vehicle or PTUPB (5 μM, 2 h) and stimulated with AFB_1-generated HepG2 tumor cell debris vs. debris alone. (*E*) Inflammatory cytokine array of conditioned media from RAW 264.7 macrophages treated with vehicle or PTUPB (5 μM, 2 h) and stimulated with LPS-generated MS-1 endothelial cell debris vs. debris alone.

To exclude that the AFB_1-generated debris-stimulated cytokine storm and its suppression via dual COX-2/sEH inhibition were specific to the RAW 264.7 macrophage cell line, we performed cytokine array screening of conditioned medium from primary human monocyte-derived macrophages stimulated with AFB_1-generated debris. Indeed, AFB_1-generated HepG2 debris also triggered a cytokine storm, including MIF/GIF/DER6, serpin E1/PAI-1, IL-8/CXCL8, and MIP-1α/MIP-1β/CCL3/CCL4 by human monocyte-derived macrophages, compared with macrophages not exposed to the debris (Fig. 2*D*). Remarkably, PTUPB prevented the cytokine storm in human monocyte-derived macrophages (Fig. 2*D*). AFB_1 exposure can increase lipopolysaccharide (LPS) levels in the liver, and LPS-stimulated inflammation can stimulate tumor dormancy escape in mice (77). LPS-generated endothelial cell debris (MS-1) stimulated a macrophage-derived cytokine storm, including MIP-1α/CCL3, MIP-1β/CCL4, MIP-2/CXCL2, G-CSF, and TNF-α, that was suppressed by PTUPB (Fig. 2*E*). Thus, the protumorigenic and proangiogenic cytokine storm triggered by carcinogen debris-stimulated macrophages was prevented by the dual COX-2/sEH inhibitor PTUPB.

Dual COX-2/sEH Inhibition Stimulates Macrophage Phagocytosis of AFB_1-Generated HCC Debris. We reasoned that since carcinogen-generated debris can promote tumor growth, clearance of debris may suppress this growth. A critical function of inflammation resolution is nonphlogistic macrophage phagocytosis of debris (20, 45, 78, 79). Thus, we next assessed macrophage phagocytosis of AFB_1-generated tumor cell debris in response to inhibition of COX-2 and/or sEH enzymes. Neither murine nor human monocyte-derived macrophage phagocytosis of AFB_1-generated Hepa 1-6 or HepG2 debris, respectively, was affected by celecoxib treatment (Fig. 3*A*), which is consistent with studies demonstrating that inflammation resolution can be impaired by COX-2 inhibition (20, 44, 45). In contrast, treatment of human monocyte-derived and primary murine peritoneal macrophages with an sEH inhibitor (TPPU) at 0.01 to 10 μM stimulated phagocytosis of AFB_1-generated human (HepG2) and murine (Hepa 1-6) HCC tumor cell debris (Fig. 3*B*). Moreover, the dual COX-2/sEH inhibitor PTUPB potently promoted RAW 264.7 and peritoneal murine macrophage phagocytosis of AFB_1-generated Hepa 1-6 tumor cell debris by 100 to 250% above vehicle (Fig. 3*C*). Thus, stimulation of the resolution of inflammation by dual COX-2/sEH inhibition not only prevents the proinflammatory cytokine storm, but also enhances macrophage phagocytosis of AFB_1-generated HCC debris.

Dual COX-2/sEH Inhibition Suppresses AFB_1 Debris-Stimulated ER Stress and an Eicosanoid Storm. Carcinogen-induced ER stress accelerates HCC via proinflammatory cytokines and caspase-activated cell death (80, 81). To determine whether carcinogen-induced cell

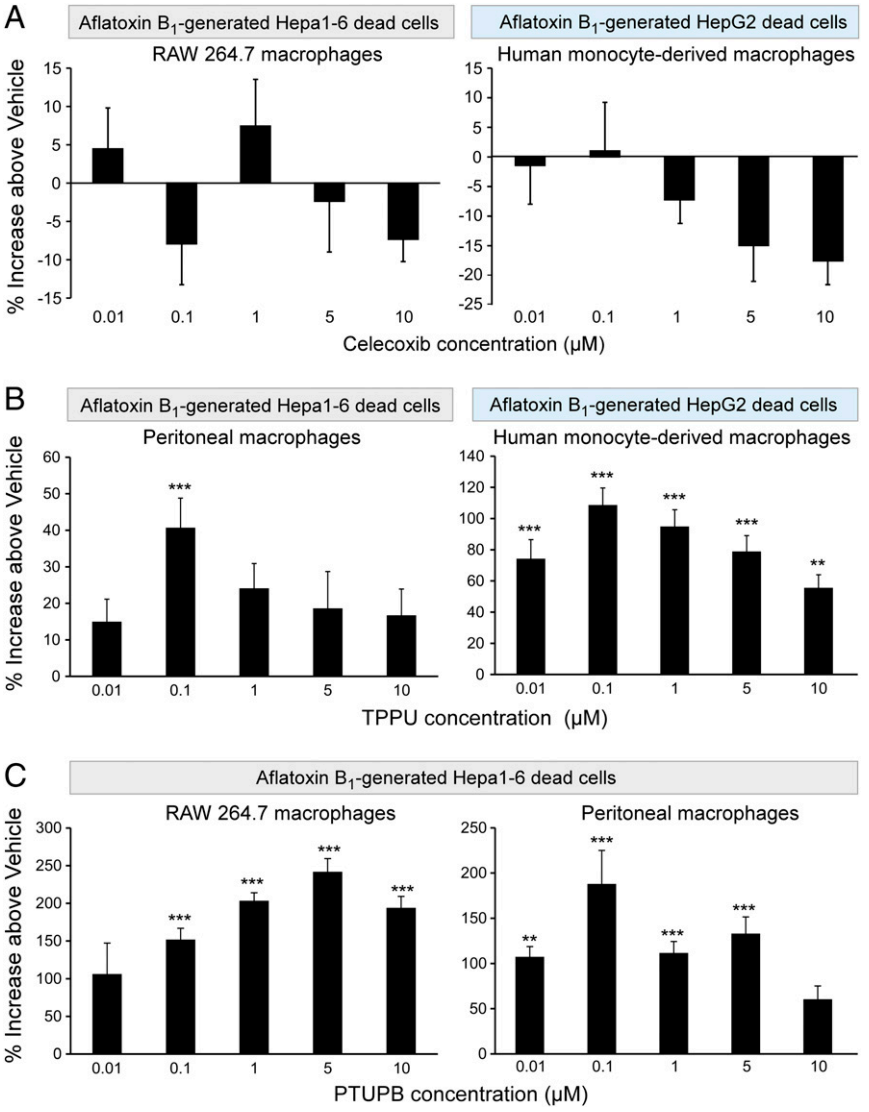

Fig. 3. Dual COX-2/sEH inhibition stimulates macrophage phagocytosis of AFB_1-generated HCC debris. Human monocyte-derived, peritoneal or RAW 264.7 murine macrophage phagocytosis of CFDA-labeled AFB_1-generated tumor cell debris measured as relative fluorescent units and normalized to percent increase above vehicle-treated macrophages. One-way ANOVA used throughout. $n = 12$ per group. $^{**}P < 0.01$, $^{***}P < 0.001$ vs. vehicle. (*A*) Celecoxib (2 h) did not stimulate RAW 264.7 (*Left*) nor human monocyte-derived (*Right*) macrophage phagocytosis of AFB_1-generated Hepa 1-6 or HepG2 debris, respectively. (*B*) sEH inhibitor (TPPU; 2 h) stimulated murine peritoneal (*Left*) and human monocyte-derived (*Right*) macrophage phagocytosis of AFB_1-generated Hepa 1-6 or HepG2 debris, respectively. (C) Dual COX-2/sEH inhibitor (PTUPB; 2 h) stimulated RAW 264.7 (*Left*) and murine peritoneal (*Right*) macrophage phagocytosis of AFB_1-generated Hepa 1-6 debris.

death stimulates ER stress, we coincubated human monocyte-derived macrophages with AFB_1-generated dead cells. AFB_1-generated HepG2 debris dramatically up-regulated the expression of ER stress-response genes in macrophages, including *CHOP*, *BiP*, and *PDI* (Fig. 4*A*). In contrast, PTUPB inhibited debris-stimulated expression of ER stress-response genes in human monocyte-derived macrophages (Fig. 4*A*). Additionally, macrophages stimulated by AFB_1-generated HepG2 debris exhibited increased protein levels of BiP and PDI, which were inhibited by PTUPB (Fig. 4*B*). Up-regulation of COX-2 protein expression by AFB_1-generated debris in human monocyte-derived macrophages was also neutralized by PTUPB to near baseline expression (Fig. 4*B*). To determine whether AFB_1-generated debris triggers the release of eicosanoids by macrophages, we performed LC-MS/MS–based oxylipin profiling of RAW 264.7 macrophages stimulated with AFB_1-generated Hepa 1-6 debris. Indeed, the debris triggered an "eicosanoid storm" of COX-derived lipid mediators, including 8-*iso*-$PGF_{2\alpha}$, PGE_2, and PGD_2 compared with macrophages not exposed to the debris or debris alone without macrophages (Fig. 4 *C* and *D* and Table 1). In contrast, PTUPB suppressed this debris-stimulated eicosanoid storm released by the macrophages and increased the LOX metabolite (20-COOH-LTB_4) as well as a COX metabolite derived from 20-HETE (20-OH-$PGF_{2\alpha}$) (Fig. 4 *C* and *D*). Interestingly, EETs (EpETrEs) and DHETs (DiHETrEs) were highly expressed in the AFB_1-generated debris (Fig. 4*D*). Thus, PTUPB potently inhibited the up-regulation of ER stress-response genes/proteins and the proinflammatory eicosanoid storm in AFB_1 debris-stimulated macrophages.

Prevention of AFB_1 Debris-Stimulated HCC and Cytokine Storm In Vivo by Dual COX-2/sEH Inhibitor PTUPB. To determine whether PTUPB suppresses carcinogen debris-stimulated HCC tumor growth, AFB_1-generated Hepa 1-6 debris was coinjected subcutaneously with a subthreshold inoculum of living Hepa 1-6 tumor cells.

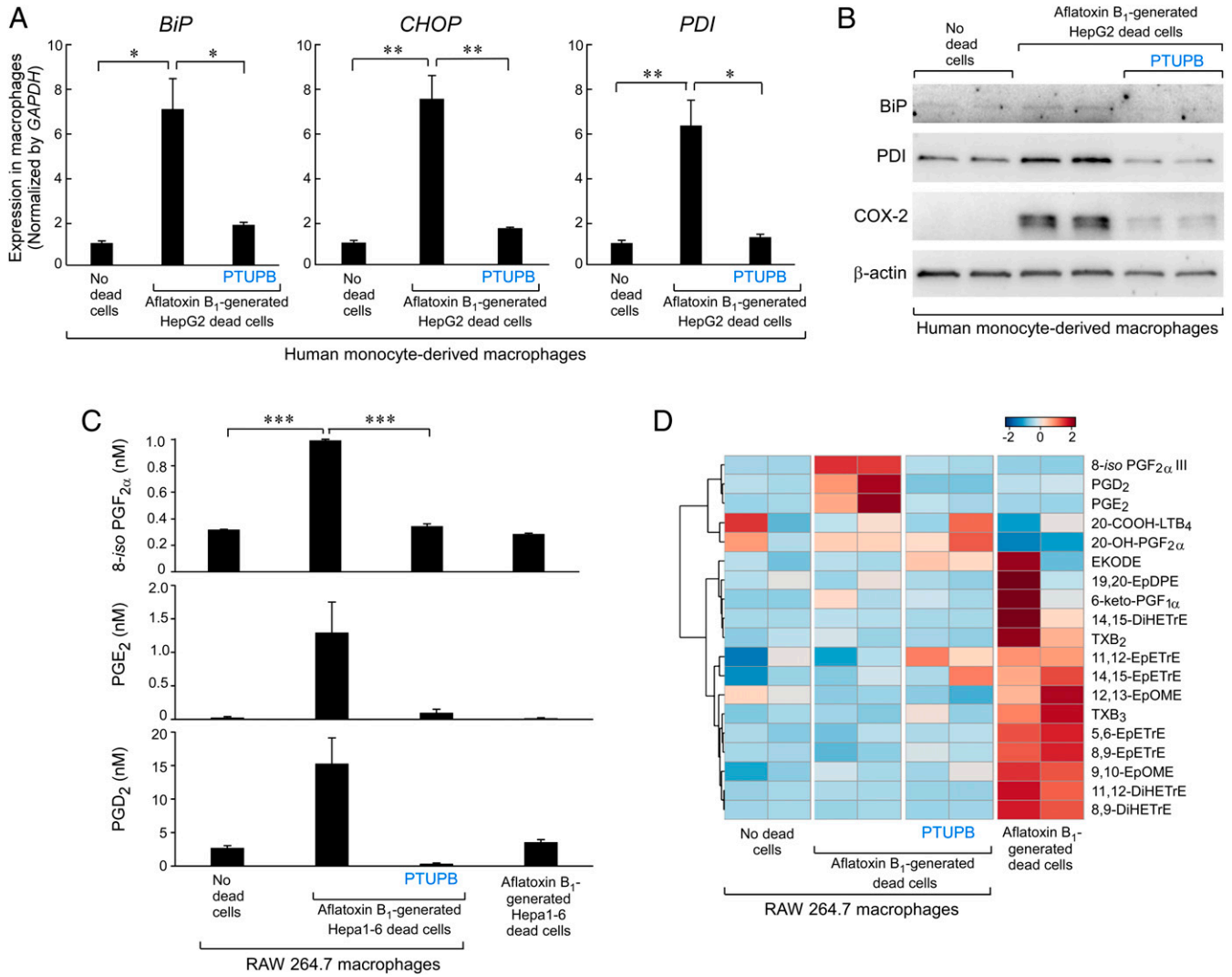

Fig. 4. Dual COX-2/sEH inhibition suppresses AFB_1 debris-stimulated ER stress and eicosanoid storm. (*A*) qPCR analysis of ER stress-response gene (*CHOP*, *BiP*, *PDI*) expression in human monocyte-derived macrophages treated with PTUPB (5 μM, 2 h) or vehicle and stimulated with AFB_1-generated HepG2 tumor cell debris. Results were normalized by *GAPDH*. $n = 3$ per group. $^*P < 0.05$, $^{**}P < 0.01$. (*B*) Western blot analysis of ER stress response (*BiP*, *PDI*) and COX-2 protein expression in human monocyte-derived macrophages treated with PTUPB (5 μM, 2 h) or vehicle and stimulated with AFB_1-generated HepG2 debris. Levels of β-actin demonstrate protein loading. $n = 2$ per group. (*C*) UPLC-MS/MS–based oxylipin analysis of RAW 264.7 macrophages treated with PTUPB (5 μM, 2 h) or vehicle and stimulated with AFB_1-generated Hepa 1-6 HCC debris or AFB_1-generated Hepa 1-6 debris alone. $n = 2$ per group. $^{***}P < 0.001$. (*D*) Heatmap of eicosanoid storm via UPLC-MS/MS–based oxylipin analysis in macrophages exposed to AFB_1-generated Hepa 1-6 HCC debris. $n = 2$ per group.

Growth of established carcinogen debris-stimulated tumors (126 to 146 mm^3) was suppressed by systemic treatment of the dual COX-2/sEH inhibitor PTUPB without overt toxicity compared to control (Fig. 5*A*). Remarkably, PTUPB also prevented debris-stimulated orthotopic HCC tumor growth and prolonged survival (Fig. 5*B*). To determine whether AFB_1-generated debris could induce a cytokine storm in vivo, we assessed the plasma for proinflammatory and proangiogenic cytokines in mice bearing debris-stimulated orthotopic HCC tumors compared to mice injected with living Hepa 1-6 cells alone or AFB_1-generated debris alone. Indeed, AFB_1 debris-stimulated tumors stimulated an in vivo cytokine storm, including increased plasma levels of BLC/CXCL13/BCA-1, TIMP-1, M-CSF, PTX-3/TSG-14, serpin E1/PAI-1, and tissue factor/coagulation factor III as compared to plasma from mice injected with living Hepa 1-6 cells alone or AFB_1-generated tumor cell debris alone (Fig. 5 *C* and *D*). Moreover, treatment with PTUPB prevented the debris-stimulated cytokine storm in vivo as compared to mice not treated with PTUPB (Fig. 5 *C* and *D*).

Discussion

Carcinogen (e.g., AFB_1)-induced cancer is a leading cause of HCC cancer death (1). Dietary aflatoxins adversely affect billions of people who are chronically exposed to a large amount of the toxin (1). Aflatoxin-induced HCC is most prevalent in developing countries due to poor postharvest management and regular consumption of food contaminated with aflatoxins (82). The incidence of HCC, the most common primary liver malignancy worldwide, is rising (83). Here, we demonstrate that AFB_1-generated and caspase-3–mediated cell death (debris) triggers HCC tumor dormancy escape via a proinflammatory eicosanoid and cytokine storm. Debris up-regulates expression of *EPHX2* (sEH) and *PTGS2* (COX-2), as well as genes involved in ER stress in macrophages, which may be contributing factors for the ensuing eicosanoid and cytokine storm. Thus, targeting a single proinflammatory mediator or eicosanoid pathway is unlikely to prevent carcinogen-induced HCC progression. Proresolving lipid mediators induce clearance of cellular debris by macrophages to

Table 1. Oxylipin analysis: Levels of eicosanoid metabolites in RAW 264.7 macrophages

	Macrophages alone	Macrophages alone	Macrophages + debris	Macrophages + debris	Macrophages + debris + PTUPB	Macrophages + debris + PTUPB	AFB_1-generated Hepa1-6 debris	AFB_1-generated Hepa1-6 debris
12,13-EpOME	1.481	1.275	0.951	1.007	0.949	0.760	1.653	2.436
9,10-EpOME	0.473	0.582	0.689	0.626	0.613	0.731	1.120	1.061
EKODE	1.480	0.208	1.462	1.148	3.778	3.226	8.590	n.d.
12,13-DiHOME	0.005	n.d.	n.d.	n.d.	n.d.	n.d.	0.091	0.074
9,10-DiHOME	n.d.	n.d.	n.d.	n.d.	n.d.	n.d.	0.017	0.021
11,12-EpETrE	0.751	0.969	0.814	0.918	1.113	1.009	1.096	1.083
14,15-EpETrE	0.763	0.840	0.825	0.874	0.849	0.996	0.962	1.031
5,6-EpETrE	12.111	10.280	9.392	12.866	12.154	12.831	26.813	29.411
8,9-EpETrE	0.917	0.905	0.748	0.854	1.052	0.946	1.632	1.786
11,12-DiHETrE	0.259	0.283	0.295	0.290	0.265	0.262	0.868	0.727
14,15-DiHETrE	0.244	0.247	0.315	0.292	0.249	0.247	1.713	0.637
5,6-DiHETrE	n.d.	n.d.	n.d.	n.d.	n.d.	n.d.	0.278	0.008
8,9-DiHETrE	0.436	0.447	0.423	0.447	0.431	0.434	1.112	0.998
19,20-EpDPE	0.586	0.688	0.533	0.713	0.561	0.510	1.483	0.604
PGD_2	3.056	2.273	11.345	19.134	0.459	0.161	3.088	3.949
PGE_2	n.d.	0.042	0.829	1.749	0.154	0.036	0.026	n.d.
8-*iso* $PGF_{2\alpha}$ III	0.321	0.317	1.001	0.984	0.363	0.327	0.292	0.280
20-COOH-LTB_4	0.695	0.303	0.394	0.472	0.361	0.640	0.262	0.442
TXB_3	43.484	62.116	58.543	44.921	101.601	52.075	174.125	241.198
20-OH-$PGF_{2\alpha}$	21.963	10.102	17.484	17.175	15.844	26.322	0.045	2.935
TXB_2	0.778	0.794	0.803	0.783	0.785	0.779	0.929	0.848
6-keto-$PGF_{1\alpha}$	2.051	2.051	2.065	2.054	2.057	2.053	2.100	2.060

Full report of concentrations (nM) of oxylipins in cell pellets is listed. UPLC-MS/MS–based oxylipin analysis in RAW 264.7 macrophages exposed to AFB_1-generated Hepa 1-6 HCC debris and/or PTUPB. $n = 2$ per group; n.d., not determined.

resolve inflammation, resulting in reduced proinflammatory cytokines (15, 20, 21, 32, 78, 79, 84). Carcinogens, including aflatoxins, disrupt inflammation resolution by impairing host-protective neutrophil and macrophage phagocytosis of debris (19, 85). Standard antiinflammatory drugs and biologics, such as steroids, nonsteroidal antiinflammatory drugs (NSAIDs), coxibs, and cytokine antagonists do not stimulate debris clearance. We now show that dual COX-2/sEH inhibition prevents AFB_1 debris-induced HCC progression by preventing the eicosanoid and cytokine storm via macrophage phagocytosis of debris and inhibition of ER stress in AFB_1 debris-stimulated macrophages.

An active stromal response in the tumor microenvironment to carcinogen-induced cytotoxicity and apoptosis supports both cell-autonomous and noncell-autonomous essential mechanisms for carcinogen-induced cancer, including the ability of a carcinogen to act as an electrophile, be genotoxic, cause genomic instability, induce epigenetic alterations, induce oxidative stress, induce chronic inflammation, be immunosuppressive, modulate receptor-mediated effects, cause immortalization, and alter cell proliferation, cell death, or angiogenesis (8, 9, 86, 87). AFB_1 is a potent liver carcinogen via genotoxic mechanisms involving formation of DNA adducts. However, genotoxic mechanisms alone may not be sufficient for carcinogenesis or increased tumor risk (4, 6), and nongenotoxic mechanisms are emerging as key characteristics of carcinogens (8, 9). Carcinogen-induced mutagenesis of normal cells leads to apoptotic cell death that creates a protumorigenic microenvironment consisting of proinflammatory mediators. Carcinogen-induced chronic inflammation in the tumor microenvironment via aberrant inflammatory cytokine release may enable cancer progression (6, 8, 9). Carcinogens such as dibenzo[*a*,*l*] pyrene can potently transform cells, even in the absence of detected DNA adducts (88). Triterpenoid oleanane, a highly potent antiinflammatory agent, prevents HCC while only partially reducing AFB_1-DNA adducts (4). Interestingly, protostane-type triterpenoids inhibit sEH (89). Inflammation is a hallmark of cancer (90) and is essential for cancer growth by oncogenes in a genetically engineered cancer model (91). Stress-induced apoptotic cell death, cytotoxicity, and inflammation caused by carcinogens, wounding, surgery, chemotherapy, and radiation can trigger activation of dormant micrometastases (33, 92). Sustained proliferative signals from cellular debris and proinflammatory cytokines in the tumor microenvironment can act synergistically with cell-autonomous mechanisms to promote tumorigenesis (15, 93). Chronic inflammation and inflammation-induced cell proliferation, oxidative stress, and reactive chemical species (e.g., ROS) potentiate DNA damage and inhibit DNA repair to drive mutations and tumor progression (24, 26, 94). Thus, there is a vicious protumorigenic feedback loop between apoptosis, inflammation, DNA damage, and carcinogenesis.

Macrophages stimulate inflammation resolution in cancer via the clearance of tumor cell debris (15, 20, 21, 32). Macrophages can phagocytose cellular debris to resolve hepatic fibrosis, a risk factor for HCC (95). However, the failure of macrophages to clear apoptotic cells results in the accumulation of debris within the tissue, which stimulates an inflammatory response that may promote cancers (15, 96). In 1956, Révész (97) demonstrated that coinjection of irradiated dead cells (debris) with tumor cells dramatically reduced the inoculum of tumor cells needed to produce tumors in rodents, which has been confirmed in multiple tumor models (12, 98–101). Tumor cell debris generated by cytotoxic cancer therapies, including chemotherapy and targeted therapy, can stimulate tumor growth (14, 15, 22). Phosphatidylserine, a marker for apoptotic cell death, activates an inflammatory feedback loop within a microenvironment that can result in a cytokine storm (15). Sterile inflammation is sustained by debris as "danger signals" (e.g., damage-associated molecular patterns) are released from dying hepatocytes that activate liver macrophages to release proangiogenic cytokines that initiate inflammation (11, 102, 103). Spontaneous apoptotic cell death rates are elevated in tumors of cancer patients that, along with the systemic inflammatory response, correlates with poor prognosis (102, 104–107). Apoptotic cell death may play a causative

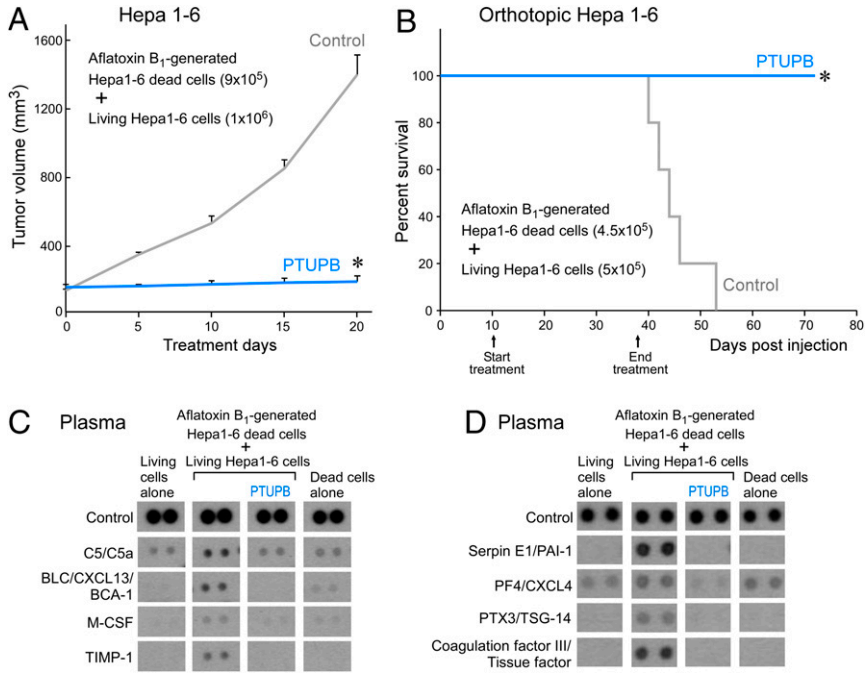

Fig. 5. Prevention of AFB_1 debris-stimulated HCC and cytokine storm in vivo by dual COX-2/sEH inhibitor PTUPB. (*A*) Tumor volume of debris-stimulated Hepa 1-6 HCC tumors systemically treated with PTUPB (30 mg/kg/d) vs. vehicle. Treatment initiated once tumors reached 100 to 200 mm^3. $n = 5$ mice per group. The two-tailed unpaired Student's *t* test was used for final tumor measurements. $*P < 0.05$. (*B*) Percent survival of mice coinjected orthotopically into the liver with AFB_1-generated Hepa 1-6 debris (4.5×10^5 dead cells) and Hepa 1-6 living cells (5×10^5). Systemic treatment with PTUPB (30 mg/kg/d) or vehicle initiated 10 d postinjection. $n = 5$ mice per group. Kaplan–Meier analysis indicated significantly prolonged survival in mice treated with PTUPB compared with control. $*P < 0.05$. (*C*) Inflammatory and (*D*) angiogenic cytokine array of plasma from control or PTUPB-treated mice bearing debris-stimulated orthotopic HCC. Plasma was collected on day 60 postinjection.

role in tumor growth providing clinical evidence of the Révész phenomenon (107–110). Stimulating the clearance of debris may not only alleviate carcinogen-induced inflammation, but also reduce carcinogen-induced DNA damage (e.g., AFB_1-DNA adduct formation). Thus, as inflammation and tissue injury resulting from carcinogen exposure can lead to the promotion of liver cancer, shifting the production of lipid mediators in the microenvironment from the proinflammatory to the proresolving type may prevent debris-stimulated tumor growth (14, 15, 33).

Aflatoxins, alcohol, hepatitis B virus, chemotherapy, and other stress-inducing carcinogens may be major risk factors for liver cancer due to their ability to induce both an eicosanoid and a cytokine storm (6). We have established an AFB_1 debris-stimulated murine tumor model applicable to other carcinogens, such as nitrosamines, polycyclic aromatic hydrocarbons, and carbon-tetrachloride. In addition, we have identified an eicosanoid and cytokine storm responsible for nongenotoxic inflammation-mediated carcinogenesis. Proinflammatory cytokines released by cell lysis stimulate inflammation via arachidonic acid-derived eicosanoids and ROS (111). Cytokine storms generate a hyperinflammatory response that may be exhibited in individuals infected with viruses such as coronavirus disease 2019 (COVID-19; SARS-CoV-2) or rheumatic diseases, and also in a subset of cancer patients that have received immunotherapy (84, 112, 113). Many of the severely ill COVID-19 patients develop a fatal "cytokine storm syndrome" (84, 112, 114). SARS-CoV-2 can activate inflammasomes in the innate immune defense system with release of proinflammatory cytokines such as IL-1 (115). The chemotherapy-induced cytokine storm may be used as a new diagnostic tool for cancer patients (23). Inflammasome activation can quickly induce an eicosanoid storm, a pathological release of bioactive lipids, including prostaglandins and leukotrienes, that rapidly initiates inflammation (116). While the eicosanoid storm is well-characterized in infection and inflammation (116, 117), further studies are required to characterize the eicosanoid storm in cancer and its modulation by various cytotoxic cancer therapies and carcinogens.

A paradigm shift has emerged in our understanding of pathological inflammation, which is now known to occur due to the loss of active resolution mechanisms (20, 45). CYP450 enzymes generate EETs, which regulate ER-stress pathways via eicosanoids and cytokines to stimulate inflammation resolution (46–48). In contrast, antiinflammatories, such as corticosteroids, coxibs, or NSAIDs, may be immunosuppressive, impair resolution, and exacerbate the cytokine storm (20, 44, 45, 114, 118). Stabilizing EETs and epoxy-fatty acids via dual COX-2/sEH inhibition suppresses proinflammatory eicosanoids and cytokines. Thus, dual COX-2/sEH eicosanoid pathway regulation is a mechanism to potently inhibit the eicosanoid and cytokine storm.

Mitochondrial dysfunction associated with oxidative and ER stress stimulates apoptosis and survival factors contributing to the persistent cycle of cell death and tissue regeneration, consistent with the "Phoenix Rising" pathway (76). Additionally, while oxidative stress, including the carcinogen-induced ER stress response, is followed by an increase in inflammatory cytokines, suppression of the unfolded protein response can inhibit multiple cytokines, including TNF-α, MCP-1, and IL-6, and thus inhibit carcinogenesis (81). Several genes have been associated as biomarkers for ER stress, including *CHOP*, *BiP*, and *PDI*. PDI is up-regulated in patients with HCC and antagonism of PDI has been shown to synergize with the commonly used HCC therapeutic sorafenib, a potent sEH inhibitor, in experimental models (57, 119). Oxidative stress may, in addition to inducing mutagenesis or cytotoxic activity, enhance survival and proliferation of cells with DNA mutations. Additionally, lipid mediators PGE_2, PGD_2, and 8-*iso*-$PGF_{2\alpha}$, a prostaglandin-like F2-isoprostane that has been used in patients as a marker for oxidative stress in inflammatory diseases (120), create a proinflammatory stress

response in the tumor microenvironment. Dietary omega-3 PUFA supplementation may enhance sorafenib therapy in HCC patients via higher levels of omega-3 epoxyeicosanoids, such as 19-20-EDP (121).

Dual COX-2/sEH inhibitors were developed by linking two pharmacophores of COX-2 and sEH inhibitors. The sEH inhibitor component blocks the cardiovascular and gastrointestinal side effects associated with NSAIDs and synergizes with the COX-2 inhibitor to reduce pain and inflammation (46, 59, 122). While these compounds inhibit both COX-2 and sEH in nanomolar ranges, their oral bioavailability is challenging for in vivo studies due to their limited water solubility, metabolic stability, and PK profile (60). sEH inhibitors are in clinical development for hypertension [Arête Therapeutics (123, 124)], chronic obstructive pulmonary disorder [GlaxoSmithKline (125–127)], and chronic pain (EicOsis Human Health). Dual COX-2/sEH inhibitors are also currently in clinical development for multiple inflammatory diseases, which can be rapidly translated to the carcinogenesis field. Our in vivo studies suggest that administration of the dual COX-2/sEH inhibitor PTUPB during and immediately after periods of high exposure to aflatoxins may prevent carcinogen-induced HCC. Dual COX-2/sEH pathway inhibition polarizes the arachidonic acid metabolism cascade from a pattern of initiation of inflammation to a pattern of resolution of inflammation. Thus, targeting the debris-mediated eicosanoid and cytokine storm via clearance of tumor debris through dual eicosanoid pathway inhibition may provide a strategy for the prevention of carcinogen-induced cancer.

Materials and Methods

Cell Culture. HepG2 human HCC cells (ATCC) were cultured in Eagle's minimum essential medium. RAW 264.7 murine macrophage cells (ATCC) and MS-1 murine endothelial cells were cultured in Dulbecco's modified eagle medium (ATCC). Hepa 1-6 (ATCC) murine HCC cells were cultured in RPMI 1640 medium (ThermoFisher). Human monocyte-derived macrophages were isolated from blood provided by healthy volunteers at the Children's Hospital Boston blood bank using density-gradient Histopaque-1077 (Sigma-Aldrich). Human monocytes were differentiated into macrophages using RPMI supplemented with 10 ng/mL GM-CSF (R&D Systems) for 7 d. Murine resident peritoneal macrophages were isolated via peritoneal gavage using sterile PBS, counted via hemocytometer, pelleted, and plated in RPMI medium. All cell culture media were supplemented with 10% FBS and 1% L-glutamine-penicillin-streptomycin (GPS) except the medium for MS-1 cells, which was supplemented with 5% FBS and 1% GPS. Cells were incubated in 5% CO_2 atmosphere at 37 °C.

Preparation of Debris. Debris was prepared by refeeding 70% confluent T150 flasks with complete media as described above containing 25 μM AFB_1 (Cayman Chemical), or 500 ng/mL LPS, and incubated for 48 or 72 h, respectively, at 37 °C. The resulting floating population was collected, pelleted, washed with PBS, counted via hemocytometer, pelleted, and resuspended in PBS at the desired concentration.

Flow Cytometry. Tumor cells were treated with 25 μM AFB_1 or vehicle (DMSO). Media containing the floating dead cell population was collected and the remaining cells were detached with trypsin and combined with the dead cells. Total cells were counted via hemocytometer, pelleted, and resuspended in PBS at 1×10^6 cells/mL. Suspensions of 2×10^5 cells were then stained with Annexin V and PI according to the Dead Cell Apoptosis Kit protocol (ThermoFisher) and assessed using BD LSR Fortessa at the Dana Farber Core and FlowJo software analysis.

qRT-PCR. Human monocyte-derived macrophage cells were treated with vehicle (DMSO) or PTUPB (5 μM) for 2 h, and then coincubated with AFB_1-generated dead cells in complete medium for 1 h. Plates were refed with serum-free medium and incubated overnight at 37 °C. The medium was decanted, the cells were washed with cold PBS, and a TRIzol reagent was added to the cells. Total RNA was isolated from the macrophages according to the manufacturer's instructions of the TRIzol reagent. The quality and quantity of the extracted RNA were measured using a Thermo Fisher Scientific NanoDrop Spectrophotometer. Isolated RNA was reverse-transcribed into cDNA using a High Capacity cDNA Reverse Transcription kit (Applied Biosystems) according to the manufacturer's instructions. qRT-PCR was analyzed by Bio-Rad CFX qPCR Instruments with Maxima SYBR-Green Master Mix (Thermo Fisher Scientific). The results of target genes were normalized to the glyceraldehyde-3-phosphate dehydrogenase (*GAPDH*) gene and compared to control cells using the $2^{-\Delta\Delta Ct}$ method. The primers of target genes were: *CHOP* (sense) 5′-GGAAACAGAGTGGTCATTCCC-3′ and (antisense) 5′-CTGCTTGAGCCGTTCATTCTC-3′, *BiP* (sense) 5′-CATCACGCCGTCCTATGTCG-3′ and (antisense) 5′-CGTCAAAGACCGTGTTCTCG-3′, *PDI* (sense) 5′-GGTGCTGCGGAAAAGCAAC-3′ and (antisense) 5′-ACCTGATCTCGGAACCTTCTG-3′, *EPHX2* (sense) 5′-GTGCTCCGAGACCGCTAAAG-3′ and (antisense) 5′-GCTGAAATCGCCTTGTCAAAGAT-3′, *PTGS2* (sense) 5′-TTCAACACACTCTATCACTGGC-3′ and (antisense) 5′-AGAAGCGTTTGCGGTACTCAT-3′, *GAPDH* (sense) 5′-ACAACTTTGGTATCGTGGAAGG-3′ and (antisense) 5′-GCCATCACGCCACAGTTTC-3′.

Western Blot.

Caspase-3 signaling. Thirty micrograms of protein from untreated living cells (control), AFB_1-treated living cells (collected from adhered population), and AFB_1-treated dead cells (collected from floating population) were run on a 4 to 12% Bis-Tris gel and transferred to a nitrocellulose membrane. Membranes were blocked in 3% BSA and incubated with caspase-3 or cleaved caspase-3 primary antibodies (1:1,000; Cell Signaling) at 4 °C overnight. The membranes were then incubated with secondary anti-rabbit or anti-mouse IgG with HRP-linked antibody for 1 h (1:3,000; Cell Signaling) and imaged using SuperSignal West Pico Chemiluminescent Substrate (ThermoFisher, catalog #34580) and film in a photo processor. Membranes were then stripped using Restore Western blot stripping buffer (ThermoFisher). β-Actin (1:5,000; Cell Signaling) was used as a loading control.

ER stress. Human monocyte-derived macrophage cells were treated with vehicle (DMSO) or PTUPB (5 μM) for 2 h, and then coincubated with AFB_1-generated dead cells in complete medium for 1 h. Plates were refed with serum-free medium and incubated overnight at 37 °C. The medium was decanted, and the cells were washed with cold PBS and lysed. The cell lysates were resolved using SDS/PAGE and transferred onto a nitrocellulose membrane. The membranes were blocked in Odyssey Blocking Buffer (LI-COR) for 1 h at room temperature and incubated with primary antibodies overnight at 4 °C. The primary antibodies used were BiP (1:1,000; Cell Signaling Technology), PDI (1:1,000; Cell Signaling Technology), COX-2 (1:1,000; Cayman Chemical), and β-actin (1:10,000; Sigma-Aldrich). The membranes were then incubated with secondary anti-rabbit or anti-mouse IgG with HRP-linked antibody for 1 h, visualized using Clarity Western ECL Substrate kit (Bio-Rad), and then detected using Bio-Rad ChemiDoc Imaging Systems.

Mouse Plasma Collection. Mice were bled retro-orbitally using microhematocrit capillary tubes (FisherBrand) into blood collection tubes with K2E (BD Biosciences) and centrifuged at 10,000 rpm at 4 °C for 10 min. Supernatant was collected in a separate tube and centrifuged at 0.2 relative centrifugal force at 4 °C for 5 min. Plasma was isolated and stored at −80 °C.

Cytokine Array and ELISA. Macrophages were plated at 1×10^6 cells per well in six-well dishes and incubated in PBS with calcium and magnesium ($PBS^{+/+}$) for 2 h at 37 °C. Plates were refed with vehicle (DMSO) or PTUPB (5 μM) in $PBS^{+/+}$ and incubated for 2 h at 37 °C. Tumor cell debris generated as described above was collected and added at a 1:4 macrophage:dead cell ratio in PBS. Debris-alone groups represent debris incubated in PBS without macrophages. After incubating for 1 h, plates were refed with serum-free medium and incubated overnight at 37 °C. Conditioned media from each well was collected and centrifuged at 1,100 rpm for 5 min to remove particulates, and then stored at −80 °C or analyzed immediately.

Conditioned media and mouse plasma were prepared and collected as described above. Samples were assessed according to each Proteome Profiler Kit or ELISA kit protocol (R&D Systems). Array control allows for comparison between membranes.

Phagocytosis Assay. Primary macrophages were plated in 96-well plates at 5×10^4 cells per well in complete RPMI medium for 18 to 24 h. Cells were refed with PBS and incubated 1 to 2 h at 37 °C prior to treatment with drugs. RAW 264.7 macrophages were plated in 96-well plates at 5×10^4 cells per well in PBS and incubated for 1 to 2 h at 37 °C. Dead cell bodies were collected, counted and fluorescently stained with carboxyfluorescein diacetate (CFDA). Macrophages were treated with vehicle, PTUPB, TPPU, or celecoxib (0.01 to 10 μM) for 2 h at 37 °C. CFDA-stained dead cell bodies (HepG2 dead cells for human monocyte-derived macrophage phagocytosis assays and Hepa 1-6 dead cells for murine peritoneal macrophage or RAW 264.7 macrophage assays) were added to 96-well plates at a 1:4 macrophage:dead cell body

ratio and incubated for 1 h at 37 °C. Plates were quenched with Trypan blue, and fluorescence was measured using a Spectra Max M5 plate reader (Molecular Devices). Relative fluorescent units were used to measure phagocytosis compared to macrophages without treatment.

Oxylipin Analysis by UPLC-MS/MS. Extraction of oxylipins from cell pellets (~5 million cells) or media was performed prior to UPLC-MS/MS analysis. For extracting lipid mediators from cell pellets, 200 μL of cold methanol was added to the cell pellets in Eppendorf tubes after addition of 10 μL of deuterated internal standards. The tubes were centrifuged for 5 min at 13,200 rpm. The supernatants were combined with another 200 μL of wash solution (ethyl acetate) and dried using speed vac. The residues were reconstituted with 100 nM CUDA methanol solution before analysis by UPLC-MS/MS; 1 mL of cell media was extracted according to previous protocol (61).

Tumor Studies. Animal studies were all reviewed and approved by the Animal Care and Use Committee of Beth Israel Deaconess Medical Center. Mice were housed at a maximum of five mice per cage in a specific pathogen-free facility with unlimited access to water and daily chow. Daily welfare evaluations and killings were performed. Six-week-old male C57BL/6 mice obtained from Jackson Laboratory were injected subcutaneously with debris and/or living tumor cells in equal volumes of PBS (100 μL per mouse). For orthotopic injections, cells were prepared as described above and injected directly into the liver of C57BL/6 mice in a volume of 20 μL per mouse. Mice were systemically treated with PTUPB (30 mg/kg/d) or vehicle (DMSO and PEG400) via mini osmotic pumps (Alzet) implanted into the peritoneum of mice on day 10 posttumor cell injection.

Statistics. Statistical analyses were performed using student's two-tailed unpaired *t* test between two groups and one-way ANOVA among more than two groups. Data are represented as mean ± SEM with *P* values less than 0.05 considered statistically significant. The Kaplan–Meier product-limit method was used to evaluate survival differences over time after the day of tumor cell injection between mice coinjected with tumor cell debris and living cells vs. living cells alone. Data are represented as percent survival with *P* values less than 0.05 considered statistically significant.

Data Availability. All data in the paper are included in the *SI Appendix*.

ACKNOWLEDGMENTS. We thank Steve Moskowitz (Advanced Medical Graphics) for preparation of the figures. This work was supported by National Institute of Environmental Health Sciences Superfund Research Program P42 ES004699 and RIVER Grant R35 ES030443-01 (to B.D.H.); Credit Unions Kids at Heart (D.P.); the Joe Andruzzi Foundation (D.P.); and the C. J. Buckley Pediatric Brain Tumor Fund (D.P.).

1. J. D. Yang *et al.*, A global view of hepatocellular carcinoma: Trends, risk, prevention and management. *Nat. Rev. Gastroenterol. Hepatol.* **16**, 589–604 (2019).
2. H. Strosnider *et al.*, Workgroup report: Public health strategies for reducing aflatoxin exposure in developing countries. *Environ. Health Perspect.* **114**, 1898–1903 (2006).
3. Y. Liu, F. Wu, Global burden of aflatoxin-induced hepatocellular carcinoma: A risk assessment. *Environ. Health Perspect.* **118**, 818–824 (2010).
4. N. M. Johnson *et al.*, Complete protection against aflatoxin B(1)-induced liver cancer with a triterpenoid: DNA adduct dosimetry, molecular signature, and genotoxicity threshold. *Cancer Prev. Res.* **7**, 658–665 (2014).
5. T. W. Kensler *et al.*, Predictive value of molecular dosimetry: Individual versus group effects of oltipraz on aflatoxin-albumin adducts and risk of liver cancer. *Cancer Epidemiol. Biomarkers Prev.* **6**, 603–610 (1997).
6. K. T. Bogen, Inflammation as a cancer co-initiator: New mechanistic model predicts low/negligible risk at noninflammatory carcinogen doses. *Dose Response* **17**, 1559325819847834 (2019).
7. M. C. Poirier, Linking DNA adduct formation and human cancer risk in chemical carcinogenesis. *Environ. Mol. Mutagen.* **57**, 499–507 (2016).
8. M. T. Smith *et al.*, Key characteristics of carcinogens as a basis for organizing data on mechanisms of carcinogenesis. *Environ. Health Perspect.* **124**, 713–721 (2016).
9. M. T. Smith *et al.*, The key characteristics of carcinogens: Relationship to the hallmarks of cancer, relevant biomarkers, and assays to measure them. *Cancer Epidemiol. Biomarkers Prev.*, 10.1158/1055-9965.EPI-19-1346 (2020).
10. M. Seehawer *et al.*, Necroptosis microenvironment directs lineage commitment in liver cancer. *Nature* **562**, 69–75 (2018).
11. L. X. Yu, Y. Ling, H. Y. Wang, Role of nonresolving inflammation in hepatocellular carcinoma development and progression. *NPJ Precis. Oncol.* **2**, 6 (2018).
12. Q. Huang *et al.*, Caspase 3-mediated stimulation of tumor cell repopulation during cancer radiotherapy. *Nat. Med.* **17**, 860–866 (2011).
13. L. Cui *et al.*, Chemotherapy induces ovarian cancer cell repopulation through the caspase 3-mediated arachidonic acid metabolic pathway. *OncoTargets Ther.* **10**, 5817–5826 (2017).
14. A. Gartung *et al.*, Suppression of chemotherapy-induced cytokine/lipid mediator surge and ovarian cancer by a dual COX-2/sEH inhibitor. *Proc. Natl. Acad. Sci. U.S.A.* **116**, 1698–1703 (2019).
15. M. L. Sulciner *et al.*, Resolvins suppress tumor growth and enhance cancer therapy. *J. Exp. Med.* **215**, 115–140 (2018).
16. D. H. Ribeiro, F. L. Ferreira, V. N. da Silva, S. Aquino, B. Corrêa, Effects of aflatoxin B(1) and fumonisin B(1) on the viability and induction of apoptosis in rat primary hepatocytes. *Int. J. Mol. Sci.* **11**, 1944–1955 (2010).
17. P. Zhu *et al.*, Aflatoxin B_1 affects apoptosis and expression of death receptor and endoplasmic reticulum molecules in chicken spleen. *Oncotarget* **8**, 99531–99540 (2017).
18. X. Peng *et al.*, Aflatoxin B1 affects apoptosis and expression of Bax, Bcl-2, and Caspase-3 in thymus and bursa of fabricius in broiler chickens. *Environ. Toxicol.* **31**, 1113–1120 (2016).
19. E. Y. Moon, D. K. Rhee, S. Pyo, Inhibition of various functions in murine peritoneal macrophages by aflatoxin B1 exposure in vivo. *Int. J. Immunopharmacol.* **21**, 47–58 (1999).
20. C. N. Serhan, Pro-resolving lipid mediators are leads for resolution physiology. *Nature* **510**, 92–101 (2014).
21. M. M. Gilligan *et al.*, Aspirin-triggered proresolving mediators stimulate resolution in cancer. *Proc. Natl. Acad. Sci. U.S.A.* **116**, 6292–6297 (2019).
22. J. Chang *et al.*, Chemotherapy-generated cell debris stimulates colon carcinoma tumor growth via osteopontin. *FASEB J.* **33**, 114–125 (2019).
23. P. S. Filippou, G. S. Karagiannis, Cytokine storm during chemotherapy: A new companion diagnostic emerges? *Oncotarget* **11**, 213–215 (2020).
24. L. B. Meira *et al.*, DNA damage induced by chronic inflammation contributes to colon carcinogenesis in mice. *J. Clin. Invest.* **118**, 2516–2525 (2008).
25. F. R. Greten *et al.*, IKKbeta links inflammation and tumorigenesis in a mouse model of colitis-associated cancer. *Cell* **118**, 285–296 (2004).
26. J. Kay, E. Thadhani, L. Samson, B. Engelward, Inflammation-induced DNA damage, mutations and cancer. *DNA Repair* **83**, 102673 (2019).
27. A. Federico, F. Morgillo, C. Tuccillo, F. Ciardiello, C. Loguercio, Chronic inflammation and oxidative stress in human carcinogenesis. *Int. J. Cancer* **121**, 2381–2386 (2007).
28. S. Reuter, S. C. Gupta, M. M. Chaturvedi, B. B. Aggarwal, Oxidative stress, inflammation, and cancer: How are they linked? *Free Radic. Biol. Med.* **49**, 1603–1616 (2010).
29. H. Hikita *et al.*, Activation of the mitochondrial apoptotic pathway produces reactive oxygen species and oxidative damage in hepatocytes that contribute to liver tumorigenesis. *Cancer Prev. Res.* **8**, 693–701 (2015).
30. D. E. Malik, R. M. David, N. J. Gooderham, Mechanistic evidence that benzo[a]pyrene promotes an inflammatory microenvironment that drives the metastatic potential of human mammary cells. *Arch. Toxicol.* **92**, 3223–3239 (2018).
31. X. Li *et al.*, Targeting of tumour-infiltrating macrophages via CCL2/CCR2 signalling as a therapeutic strategy against hepatocellular carcinoma. *Gut* **66**, 157–167 (2017).
32. Y. Ye *et al.*, Anti-cancer and analgesic effects of resolvin D2 in oral squamous cell carcinoma. *Neuropharmacology* **139**, 182–193 (2018).
33. D. Panigrahy *et al.*, Preoperative stimulation of resolution and inflammation blockade eradicates micrometastases. *J. Clin. Invest.* **129**, 2964–2979 (2019).
34. S. K. Sandhu *et al.*, A first-in-human, first-in-class, phase I study of carlumab (CNTO 888), a human monoclonal antibody against CC-chemokine ligand 2 in patients with solid tumors. *Cancer Chemother. Pharmacol.* **71**, 1041–1050 (2013).
35. C. S. Milagre *et al.*, Adaptive upregulation of EGFR limits attenuation of tumor growth by neutralizing IL6 antibodies, with implications for combined therapy in ovarian cancer. *Cancer Res.* **75**, 1255–1264 (2015).
36. M. Z. Ratajczak, M. Suszynska, M. Kucia, Does it make sense to target one tumor cell chemotactic factor or its receptor when several chemotactic axes are involved in metastasis of the same cancer? *Clin. Transl. Med.* **5**, 28 (2016).
37. A. S. Hamy *et al.*, Celecoxib with neoadjuvant chemotherapy for breast cancer might worsen outcomes differentially by COX-2 expression and ER status: Exploratory analysis of the REMAGUS02 trial. *J. Clin. Oncol.* **37**, 624–635 (2019).
38. J. F. Flamiatos *et al.*, Cyclooxygenase-2 (COX-2) inhibition for prostate cancer chemoprevention: Double-blind randomised study of pre-prostatectomy celecoxib or placebo. *BJU Int.* **119**, 709–716 (2017).
39. M. J. Edelman *et al.*, Randomized, double-blind, placebo-controlled, multicenter phase II study of the efficacy and safety of apricoxib in combination with either docetaxel or pemetrexed in patients with biomarker-selected non-small-cell lung cancer. *J. Clin. Oncol.* **33**, 189–194 (2015).
40. I. Csiki *et al.*, Targeting cyclooxygenase-2 in recurrent non-small cell lung cancer: A phase II trial of celecoxib and docetaxel. *Clin. Cancer Res.* **11**, 6634–6640 (2005).
41. H. J. Groen *et al.*, Randomized, placebo-controlled phase III study of docetaxel plus carboplatin with celecoxib and cyclooxygenase-2 expression as a biomarker for patients with advanced non-small-cell lung cancer: The NVALT-4 study. *J. Clin. Oncol.* **29**, 4320–4326 (2011).
42. S. W. Park, D. S. Heo, M. W. Sung, The shunting of arachidonic acid metabolism to 5-lipoxygenase and cytochrome p450 epoxygenase antagonizes the anti-cancer effect of cyclooxygenase-2 inhibition in head and neck cancer cells. *Cell. Oncol.* **35**, 1–8 (2012).

43. R. Ganesh, D. J. Marks, K. Sales, M. C. Winslet, A. M. Seifalian, Cyclooxygenase/lipoxygenase shunting lowers the anti-cancer effect of cyclooxygenase-2 inhibition in colorectal cancer cells. *World J. Surg. Oncol.* **10**, 200 (2012).
44. D. W. Gilroy *et al*., Inducible cyclooxygenase may have anti-inflammatory properties. *Nat. Med.* **5**, 698–701 (1999).
45. C. N. Serhan, B. D. Levy, Resolvins in inflammation: Emergence of the pro-resolving superfamily of mediators. *J. Clin. Invest.* **128**, 2657–2669 (2018).
46. J. D. Imig, B. D. Hammock, Soluble epoxide hydrolase as a therapeutic target for cardiovascular diseases. *Nat. Rev. Drug Discov.* **8**, 794–805 (2009).
47. D. W. Gilroy *et al*., CYP450-derived oxylipins mediate inflammatory resolution. *Proc. Natl. Acad. Sci. U.S.A.* **113**, E3240–E3249 (2016).
48. J. Bystrom *et al*., Inducible CYP2J2 and its product 11,12-EET promotes bacterial phagocytosis: A role for CYP2J2 deficiency in the pathogenesis of Crohn's disease? *PLoS One* **8**, e75107 (2013).
49. K. Node *et al*., Anti-inflammatory properties of cytochrome P450 epoxygenase-derived eicosanoids. *Science* **285**, 1276–1279 (1999).
50. D. C. Zeldin, Epoxygenase pathways of arachidonic acid metabolism. *J. Biol. Chem.* **276**, 36059–36062 (2001).
51. B. A. Flitter *et al*., Pseudomonas aeruginosa sabotages the generation of host pro-resolving lipid mediators. *Proc. Natl. Acad. Sci. U.S.A.* **114**, 136–141 (2017).
52. A. Planagumà *et al*., Lovastatin decreases acute mucosal inflammation via 15-epi-lipoxin A4. *Mucosal Immunol.* **3**, 270–279 (2010).
53. K. R. Schmelzer *et al*., Soluble epoxide hydrolase is a therapeutic target for acute inflammation. *Proc. Natl. Acad. Sci. U.S.A.* **102**, 9772–9777 (2005).
54. E. Ono *et al*.; National Heart, Lung, and Blood Institute's Asthma Clinical Research Network, Lipoxin generation is related to soluble epoxide hydrolase activity in severe asthma. *Am. J. Respir. Crit. Care Med.* **190**, 886–897 (2014).
55. M. Rodriguez, M. Clare-Salzler, Eicosanoid imbalance in the NOD mouse is related to a dysregulation in soluble epoxide hydrolase and 15-PGDH expression. *Ann. N. Y. Acad. Sci.* **1079**, 130–134 (2006).
56. T. R. Harris *et al*., Inhibition of soluble epoxide hydrolase attenuates hepatic fibrosis and endoplasmic reticulum stress induced by carbon tetrachloride in mice. *Toxicol. Appl. Pharmacol.* **286**, 102–111 (2015).
57. J. Y. Liu *et al*., Sorafenib has soluble epoxide hydrolase inhibitory activity, which contributes to its effect profile in vivo. *Mol. Cancer Ther.* **8**, 2193–2203 (2009).
58. C. Li *et al*., Sorafenib attenuated the function of natural killer cells infiltrated in HCC through inhibiting ERK1/2. *Int. Immunopharmacol.* **76**, 105855 (2019).
59. K. R. Schmelzer *et al*., Enhancement of antinociception by coadministration of nonsteroidal anti-inflammatory drugs and soluble epoxide hydrolase inhibitors. *Proc. Natl. Acad. Sci. U.S.A.* **103**, 13646–13651 (2006).
60. S. H. Hwang *et al*., Synthesis and structure-activity relationship studies of urea-containing pyrazoles as dual inhibitors of cyclooxygenase-2 and soluble epoxide hydrolase. *J. Med. Chem.* **54**, 3037–3050 (2011).
61. G. Zhang *et al*., Dual inhibition of cyclooxygenase-2 and soluble epoxide hydrolase synergistically suppresses primary tumor growth and metastasis. *Proc. Natl. Acad. Sci. U.S.A.* **111**, 11127–11132 (2014).
62. Y. F. Zhang *et al*., A COX-2/sEH dual inhibitor PTUPB ameliorates cecal ligation and puncture-induced sepsis in mice via anti-inflammation and anti-oxidative stress. *Biomed. Pharmacother.* **126**, 109907 (2020).
63. C. C. Sun *et al*., PTUPB ameliorates high-fat diet-induced non-alcoholic fatty liver disease via inhibiting NLRP3 inflammasome activation in mice. *Biochem. Biophys. Res. Commun.* **523**, 1020–1026 (2020).
64. C. Y. Zhang *et al*., COX-2/sEH dual inhibitor PTUPB alleviates bleomycin-induced pulmonary fibrosis in mice via inhibiting senescence. *FEBS J.* **287**, 1666–1680 (2020).
65. N. Lakkappa *et al*., Evaluation of antiparkinson activity of PTUPB by measuring dopamine and its metabolites in Drosophila melanogaster: LC-MS/MS method development. *J. Pharm. Biomed. Anal.* **149**, 457–464 (2018).
66. M. Dileepan *et al*., Effect of dual sEH/COX-2 inhibition on allergen-induced airway inflammation. *Front. Pharmacol.* **10**, 1118 (2019).
67. M. A. Hye Khan *et al*., A dual COX-2/sEH inhibitor improves the metabolic profile and reduces kidney injury in Zucker diabetic fatty rat. *Prostaglandins Other Lipid Mediat.* **125**, 40–47 (2016).
68. F. Wang *et al*., COX-2/sEH dual inhibitor PTUPB potentiates the antitumor efficacy of cisplatin. *Mol. Cancer Ther.* **17**, 474–483 (2018).
69. Q. M. Anstee, H. L. Reeves, E. Kotsiliti, O. Govaere, M. Heikenwalder, From NASH to HCC: Current concepts and future challenges. *Nat. Rev. Gastroenterol. Hepatol.* **16**, 411–428 (2019).
70. H. Liu *et al*., Colorectal cancer is associated with a deficiency of lipoxin A_4, an endogenous anti-inflammatory mediator. *J. Cancer* **10**, 4719–4730 (2019).
71. J. Schnittert, M. A. Heinrich, P. R. Kuninty, G. Storm, J. Prakash, Reprogramming tumor stroma using an endogenous lipid lipoxin A4 to treat pancreatic cancer. *Cancer Lett.* **420**, 247–258 (2018).
72. J. P. Cata *et al*., Inflammation and pro-resolution inflammation after hepatobiliary surgery. *World J. Surg. Oncol.* **15**, 152 (2017).
73. L. Stenke, C. Edenius, J. Samuelsson, J. A. Lindgren, Deficient lipoxin synthesis: A novel platelet dysfunction in myeloproliferative disorders with special reference to blastic crisis of chronic myelogenous leukemia. *Blood* **78**, 2989–2995 (1991).
74. Ö. Gül-Utku *et al*., The role of resolvin D1 in the differential diagnosis of the cholangiocarcinoma and benign biliary diseases. *Clin. Lab.*, 10.7754/Clin.Lab.2020.200212 (2020).
75. M. L. Sulciner, A. Gartung, M. M. Gilligan, C. N. Serhan, D. Panigrahy, Targeting lipid mediators in cancer biology. *Cancer Metastasis Rev.* **37**, 557–572 (2018).
76. F. Li *et al*., Apoptotic cells activate the "phoenix rising" pathway to promote wound healing and tissue regeneration. *Sci. Signal.* **3**, ra13 (2010).
77. J. Albrengues *et al*., Neutrophil extracellular traps produced during inflammation awaken dormant cancer cells in mice. *Science* **361**, eaao4227 (2018).
78. N. Chiang *et al*., Infection regulates pro-resolving mediators that lower antibiotic requirements. *Nature* **484**, 524–528 (2012).
79. M. Spite *et al*., Resolvin D2 is a potent regulator of leukocytes and controls microbial sepsis. *Nature* **461**, 1287–1291 (2009).
80. I. Tabas, D. Ron, Integrating the mechanisms of apoptosis induced by endoplasmic reticulum stress. *Nat. Cell Biol.* **13**, 184–190 (2011).
81. Y. P. Vandewynckel *et al*., Tauroursodeoxycholic acid dampens oncogenic apoptosis induced by endoplasmic reticulum stress during hepatocarcinogen exposure. *Oncotarget* **6**, 28011–28025 (2015).
82. M. C. Kew, Aflatoxins as a cause of hepatocellular carcinoma. *J. Gastrointestin. Liver Dis.* **22**, 305–310 (2013).
83. P. Dasgupta *et al*., Global trends in incidence rates of primary adult liver cancers: A systematic review and meta-analysis. *Front. Oncol.* **10**, 171 (2020).
84. D. Panigrahy *et al*., Inflammation resolution: A dual-pronged approach to averting cytokine storms in COVID-19? *Cancer Metastasis Rev.* **39**, 337–340 (2020).
85. J. Mehrzad *et al*., In vitro effects of very low levels of aflatoxin B_1 on free radicals production and bactericidal activity of bovine blood neutrophils. *Vet. Immunol. Immunopathol.* **141**, 16–25 (2011).
86. A. O. Pisco, S. Huang, Non-genetic cancer cell plasticity and therapy-induced stemness in tumour relapse: "What does not kill me strengthens me". *Br. J. Cancer* **112**, 1725–1732 (2015).
87. G. S. Karagiannis *et al*., Neoadjuvant chemotherapy induces breast cancer metastasis through a TMEM-mediated mechanism. *Sci. Transl. Med.* **9**, eaan0026 (2017).
88. S. Nesnow *et al*., Comparison of the morphological transforming activities of dibenzo[a,l]pyrene and benzo[a]pyrene in C3H10T1/2CL8 cells and characterization of the dibenzo[a,l]pyrene-DNA adducts. *Carcinogenesis* **18**, 1973–1978 (1997).
89. C. P. Sun *et al*., Protostane-type triterpenoids as natural soluble epoxide hydrolase inhibitors: Inhibition potentials and molecular dynamics. *Bioorg. Chem.* **96**, 103637 (2020).
90. A. Mantovani, Cancer: Inflaming metastasis. *Nature* **457**, 36–37 (2009).
91. C. Guerra *et al*., Chronic pancreatitis is essential for induction of pancreatic ductal adenocarcinoma by K-Ras oncogenes in adult mice. *Cancer Cell* **11**, 291–302 (2007).
92. J. A. Krall *et al*., The systemic response to surgery triggers the outgrowth of distant immune-controlled tumors in mouse models of dormancy. *Sci. Transl. Med.* **10**, eaan3464 (2018).
93. A. M. De Marzo *et al*., Inflammation in prostate carcinogenesis. *Nat. Rev. Cancer* **7**, 256–269 (2007).
94. O. Kiraly, G. Gong, W. Olipitz, S. Muthupalani, B. P. Engelward, Inflammation-induced cell proliferation potentiates DNA damage-induced mutations in vivo. *PLoS Genet.* **11**, e1004901 (2015).
95. Y. Watanabe *et al*., Mesenchymal stem cells and induced bone marrow-derived macrophages synergistically improve liver fibrosis in mice. *Stem Cells Transl. Med.* **8**, 271–284 (2019).
96. R. B. Birge *et al*., Phosphatidylserine is a global immunosuppressive signal in efferocytosis, infectious disease, and cancer. *Cell Death Differ.* **23**, 962–978 (2016).
97. L. Révész, Effect of tumour cells killed by X-rays upon the growth of admixed viable cells. *Nature* **178**, 1391–1392 (1956).
98. R. Chaurio *et al*., UVB-irradiated apoptotic cells induce accelerated growth of co-implanted viable tumor cells in immune competent mice. *Autoimmunity* **46**, 317–322 (2013).
99. C. A. Ford *et al*., Oncogenic properties of apoptotic tumor cells in aggressive B cell lymphoma. *Curr. Biol.* **25**, 577–588 (2015).
100. P. M. Gunjal *et al*., Evidence for induction of a tumor metastasis-receptive microenvironment for ovarian cancer cells in bone marrow and other organs as an unwanted and underestimated side effect of chemotherapy/radiotherapy. *J. Ovarian Res.* **8**, 20 (2015).
101. I. A. da Silva Jr., R. Chammas, A. P. Lepique, S. Jancar, Platelet-activating factor (PAF) receptor as a promising target for cancer cell repopulation after radiotherapy. *Oncogenesis* **6**, e296 (2017).
102. R. S. Kornbluth, The immunological potential of apoptotic debris produced by tumor cells and during HIV infection. *Immunol. Lett.* **43**, 125–132 (1994).
103. M. Chen *et al*., High-mobility group box 1 promotes hepatocellular carcinoma progression through miR-21-mediated matrix metalloproteinase activity. *Cancer Res.* **75**, 1645–1656 (2015).
104. A. H. Wyllie, The biology of cell death in tumours. *Anticancer Res.* **5**, 131–136 (1985).
105. J. S. de Jong, P. J. van Diest, J. P. Baak, Number of apoptotic cells as a prognostic marker in invasive breast cancer. *Br. J. Cancer* **82**, 368–373 (2000).
106. B. Sun *et al*., Extent, relationship and prognostic significance of apoptosis and cell proliferation in synovial sarcoma. *Eur. J. Cancer Prev.* **15**, 258–265 (2006).
107. C. D. Gregory, J. D. Pound, Cell death in the neighbourhood: Direct microenvironmental effects of apoptosis in normal and neoplastic tissues. *J. Pathol.* **223**, 177–194 (2011).
108. K. N. Naresh, K. Lakshminarayanan, S. A. Pai, A. M. Borges, Apoptosis index is a predictor of metastatic phenotype in patients with early stage squamous carcinoma of the tongue: A hypothesis to support this paradoxical association. *Cancer* **91**, 578–584 (2001).
109. M. Jalalinadoushan, H. Peivareh, A. Azizzadeh Delshad, Correlation between apoptosis and histological grade of transitional cell carcinoma of urinary bladder. *Urol. J.* **1**, 177–179 (2004).
110. J. Alcaide *et al*., The role and prognostic value of apoptosis in colorectal carcinoma. *BMC Clin. Pathol.* **13**, 24 (2013).
111. M. Soares, G. A. Feres, J. I. Salluh, Systemic inflammatory response syndrome and multiple organ dysfunction in patients with acute tumor lysis syndrome. *Clinics* **64**, 479–481 (2009).

112. C. Huang *et al*., Clinical features of patients infected with 2019 novel coronavirus in Wuhan, China. *Lancet* **395**, 497–506 (2020).
113. R. Q. Cron, W. W. Chatham, The rheumatologist's role in covid-19. *J. Rheumatol.* **47**, 639–642 (2020).
114. P. Mehta *et al*.; HLH Across Speciality Collaboration, UK, COVID-19: Consider cytokine storm syndromes and immunosuppression. *Lancet* **395**, 1033–1034 (2020).
115. H. Zhang, J. M. Penninger, Y. Li, N. Zhong, A. S. Slutsky, Angiotensin-converting enzyme 2 (ACE2) as a SARS-CoV-2 receptor: Molecular mechanisms and potential therapeutic target. *Intensive Care Med.* **46**, 586–590 (2020).
116. J. von Moltke *et al*., Rapid induction of inflammatory lipid mediators by the inflammasome in vivo. *Nature* **490**, 107–111 (2012).
117. E. A. Dennis, P. C. Norris, Eicosanoid storm in infection and inflammation. *Nat. Rev. Immunol.* **15**, 511–523 (2015).
118. C. D. Russell, J. E. Millar, J. K. Baillie, Clinical evidence does not support corticosteroid treatment for 2019-nCoV lung injury. *Lancet* **395**, 473–475 (2020).
119. J. K. Won *et al*., Protein disulfide isomerase inhibition synergistically enhances the efficacy of sorafenib for hepatocellular carcinoma. *Hepatology* **66**, 855–868 (2017).
120. R. Dworski *et al*., Assessment of oxidant stress in allergic asthma by measurement of the major urinary metabolite of F2-isoprostane, 15-F2t-IsoP (8-iso-PGF2alpha). *Clin. Exp. Allergy* **31**, 387–390 (2001).
121. C. G. Leineweber *et al*., Assessment of the effect of sorafenib on omega-6 and omega-3 epoxyeicosanoid formation in patients with hepatocellular carcinoma. *Int. J. Mol. Sci.* **21**, E1875 (2020).
122. S. K. Goswami *et al*., Pharmacological inhibition of soluble epoxide hydrolase or genetic deletion reduces diclofenac-induced gastric ulcers. *Life Sci.* **180**, 114–122 (2017).
123. H. C. Shen, B. D. Hammock, Discovery of inhibitors of soluble epoxide hydrolase: A target with multiple potential therapeutic indications. *J. Med. Chem.* **55**, 1789–1808 (2012).
124. S. D. Kodani, B. D. Hammock, The 2014 Bernard B. Brodie award lecture-epoxide hydrolases: Drug metabolism to therapeutics for chronic pain. *Drug Metab. Dispos.* **43**, 788–802 (2015).
125. P. L. Podolin *et al*., In vitro and in vivo characterization of a novel soluble epoxide hydrolase inhibitor. *Prostaglandins Other Lipid Mediat.* **104–105**, 25–31 (2013).
126. A. L. Lazaar *et al*., Pharmacokinetics, pharmacodynamics and adverse event profile of GSK2256294, a novel soluble epoxide hydrolase inhibitor. *Br. J. Clin. Pharmacol.* **81**, 971–979 (2016).
127. S. L. Belyanskaya, Y. Ding, J. F. Callahan, A. L. Lazaar, D. I. Israel, Discovering drugs with DNA-encoded library technology: From concept to clinic with an inhibitor of soluble epoxide hydrolase. *ChemBioChem* **18**, 837–842 (2017).